AirSWOT measurements of river water surface elevation and slope: Tanana River, AK

Elizabeth H. Altenau[1] [iD], Tamlin M. Pavelsky[1] [iD], Delwyn Moller[2], Christine Lion[1], Lincoln H. Pitcher[3] [iD], George H. Allen[1] [iD], Paul D. Bates[4] [iD], Stéphane Calmant[5], Michael Durand[6] [iD], and Laurence C. Smith[3] [iD]

[1]Department of Geological Sciences, University of North Carolina at Chapel Hill, Chapel Hill, North Carolina, USA, [2]Remote Sensing Solutions, Inc., Pasadena, California, USA, [3]Department of Geography, University of California, Los Angeles, California, USA, [4]School of Geographical Sciences, University of Bristol, Bristol, UK, [5]Laboratoire d'Etudes en Géophysique et Océanographie Spatiale, UMR 5566, CNES/CNRS/IRD/Université de Toulouse, Observatoire Midi-Pyrénées, Toulouse, France, [6]School of Earth Science and Byrd Polar and Climate Research Center, Ohio State University, Columbus, Ohio, USA

Abstract Fluctuations in water surface elevation (WSE) along rivers have important implications for water resources, flood hazards, and biogeochemical cycling. However, current in situ and remote sensing methods exhibit key limitations in characterizing spatiotemporal hydraulics of many of the world's river systems. Here we analyze new measurements of river WSE and slope from AirSWOT, an airborne analogue to the Surface Water and Ocean Topography (SWOT) mission aimed at addressing limitations in current remotely sensed observations of surface water. To evaluate its capabilities, we compare AirSWOT WSEs and slopes to in situ measurements along the Tanana River, Alaska. Root-mean-square error is 9.0 cm for WSEs averaged over 1 km^2 areas and 1.0 cm/km for slopes along 10 km reaches. Results indicate that AirSWOT can accurately reproduce the spatial variations in slope critical for characterizing reach-scale hydraulics. AirSWOT's high-precision measurements are valuable for hydrologic analysis, flood modeling studies, and for validating future SWOT measurements.

1. Introduction

Rivers play a critical role in Earth's water cycle by transporting surface runoff to the oceans. In doing so, they provide key ecological habitat, play an important part in nutrient cycling, act as navigation pathways for trade and recreation, and help sustain human life as sources of fresh water. Research over the past several decades reveals a growing urgency to monitor the globe's spatial and temporal surface water fluxes as they adjust to climate change [*Famiglietti and Rodell*, 2013; *Bates et al.*, 2014; *Clark et al.*, 2015; *Rodell et al.*, 2015]. However, existing in situ and remote sensing methods for measuring rivers and lakes have limitations that prevent a consistent and comprehensive view of global-scale surface water dynamics [*Alsdorf et al.*, 2007b; *Schumann et al.*, 2009; *Bates*, 2012].

Remote sensing technology provides intriguing new ways to address the limitations of in situ observations, which often fail during overbank flows and are unavailable in many parts of the globe [*Hannah et al.*, 2011; *Di Baldassarre and Uhlenbrook*, 2012]. Optical sensors such as Landsat and SPOT can accurately observe inundation extent, but they cannot measure WSEs and are limited by clouds and darkness [*Marcus and Fonstad*, 2008]. Several types of active radars overcome the drawbacks of optical sensors, although all current systems also have limitations of their own [*Smith*, 1997; *Calmant et al.*, 2008; *Schumann et al.*, 2009]. Radar altimetry measurements from sensors such as Jason-2 and Envisat provide point-based measurements of river WSEs, which can be used to interpolate slopes and develop stage-discharge relationships [*O'Loughlin et al.*, 2013; *Paris et al.*, 2016]. However, altimeter observations have low spatial and temporal resolutions, with vertical errors of decimeters to meters [*Calmant et al.*, 2008; *Biancamaria et al.*, 2016a; *O'Loughlin et al.*, 2016]. Interferometric synthetic aperture radar (InSAR) images can recover WSE changes under inundated vegetation, but existing spaceborne InSARs cannot ordinarily retrieve WSEs over open water [*Alsdorf et al.*, 2007a]. Therefore, current remotely sensed measurements of WSEs and slopes are constrained by resolutions and accuracies that limit the visibility of surface waters at global scales [*Alsdorf et al.*, 2007b; *Bates*, 2012; *Garambois et al.*, 2016].

The Surface Water and Ocean Topography (SWOT) mission aims to address the principal limitations of remote sensing for estimating surface water fluxes [*Biancamaria et al.*, 2016b]. SWOT is expected to provide

simultaneous, 2D measurements of WSEs for many of the world's prominent rivers, lakes, and wetlands, with decimeter-level accuracy over 1 km^2 areas [*Pavelsky et al.*, 2014]. *Biancamaria et al.* [2016b] provides further information regarding the capabilities and limitations of SWOT to measure rivers and lakes. AirSWOT, an airborne instrument that produces radar measurements analogous to (but not identical to) SWOT, was designed to assess sensor capabilities, develop algorithms, and eventually validate SWOT measurements. Unlike SWOT, AirSWOT provides an opportunity to explore important questions regarding river hydraulics at spatial and temporal resolutions unattainable by satellites. To date, however, there has been no published evaluation of AirSWOT's ability to accurately measure these important hydrologic variables or the spatial scales required for averaging the data in order to meet the proposed accuracies.

Here we present analysis of new measurements of river WSE and slope acquired on 9 June 2015 during an AirSWOT campaign over the Tanana River, Alaska. The objectives of this study are (1) to determine the WSE and slope errors associated with AirSWOT measurements of rivers, (2) to evaluate AirSWOT's effectiveness as a validation instrument for the SWOT hydrology measurements, and (3) to explore whether AirSWOT's measurements are precise enough to capture centimeter-per-kilometer-scale variations in river slope, which are critical for characterizing reach-scale river hydraulics. More detailed measurements of WSE and slope are needed to understand the primary factors controlling slope variability along river systems, which are essential for predicting floods and for defining reaches used to estimate discharge from remotely sensed data [*Durand et al.*, 2016; *Garambois et al.*, 2016].

2. AirSWOT

The AirSWOT payload comprises a multibaseline Ka-band InSAR, a state-of-the-art inertial measurement unit (Applianix 610), and a three-band color infrared (CIR) camera [http://cirrus-designs.com/]. These sensors are operated from a NASA B200 aircraft typically at an altitude of 8230 m above sea level. AirSWOT's Ka-band InSAR has multiple temporal and cross-track baselines in order to characterize the scattering and statistics expected from the primary instrument on SWOT (the Ka-band Radar Interferometer or KaRIN [*Enjolras and Rodriguez*, 2009; *Biancamaria et al.*, 2016b]), provide data for developing classification algorithms, and improve the understanding of the instrument performance and limitations over the large variety of landscape conditions that SWOT will observe (i.e., sea ice, water obscured by vegetation, and frozen or partially frozen rivers). AirSWOT is designed with high-accuracy elevation mapping capabilities and a swath mode that enables mapping of entire river networks in a reasonable timeframe. Further description of system parameters and calibration/validation requirements of AirSWOT's InSAR are presented by *Moller et al.* [2011].

It is important to note the difference between the two separate observation swaths collected by the AirSWOT Ka-band InSAR. The inner swath has incidence angles ranging from 0 to 6°, which fully encompasses KaRIN incidence angles of 0.6–3.9° [*Fjørtoft et al.*, 2014], while the outer swath has incidence angles ranging from 4 to 25°. When data are collected from ~8200 m, the inner swath is approximately 800 m in width, while the outer swath covers ~4 km. In this paper, we exclusively assess data from the wider outer swath because robust methods have not yet been developed to process data from the inner swath. Differences in incidence angles and viewing geometry render AirSWOT's observations substantially different from anticipated SWOT observations. While the random elevation errors of AirSWOT's outer swath should be smaller than what could be achieved by SWOT [*Fu et al.*, 2012], the SWOT platform will have superior stability compared to AirSWOT and SWOT incidence angles will likely produce better signal-to-noise ratios compared to AirSWOT's outer swath. Nonetheless, because AirSWOT's outer swath is designed to produce highly accurate WSE measurements it is likely to be useful for validating SWOT WSE measurements.

In preparation for the SWOT mission, the scientific community has identified WSE and slope accuracies needed for executing robust science of global surface water dynamics, which we use as a baseline to assess AirSWOT's performance and suitability as a validation instrument and its capabilities to provide useful hydraulic measurements in its own right. These accuracies are ±10 cm or better for WSEs when averaged over 1 km^2 areas and ±1.7 cm/km for slopes after processing along a maximum of 10 km of flow distance [*Biancamaria et al.*, 2016b; *Rodriguez*, 2016]. Primary sources of error for AirSWOT likely include layover from high topography and vegetation, random noise, and elements of the processing methodology such as the estimation of ambiguity height in phase unwrapping [*Rosen et al.*, 2000].
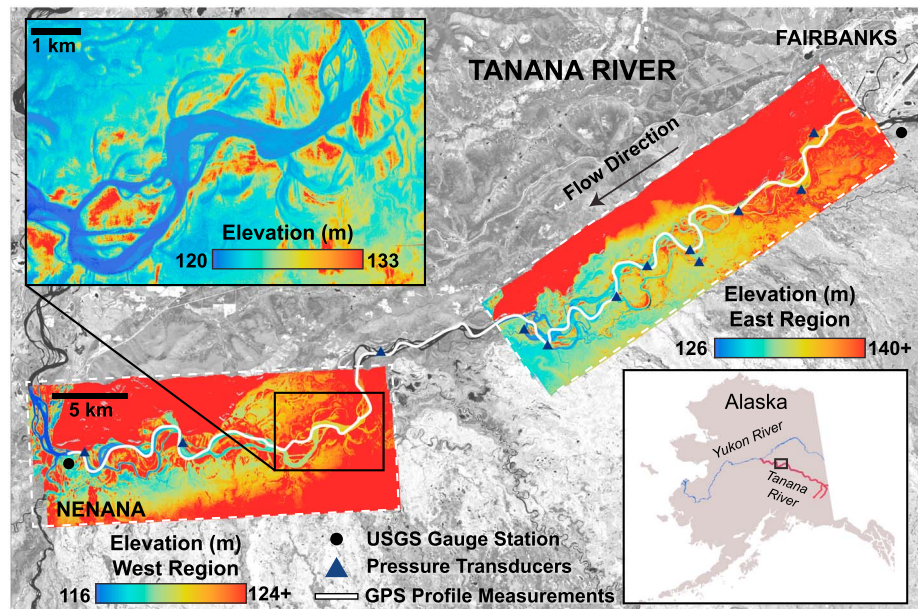
Figure 1. Location of the Tanana River study reach shown using a Landsat 8 near-infrared image acquired on 18/6/2013. AirSWOT elevation measurements and extent from 9 June 2015 are shown in the white dashed boxes.

3. Study Site

For this study, we chose an ~90 km reach of the Tanana River, Alaska, bounded by two U.S. Geological Survey (USGS) gauge stations in the towns of Fairbanks and Nenana (Figure 1). This site is ideal for assessment of AirSWOT's capabilities to measure WSEs and slopes over a highly dynamic, multichannel river. The shape of the annual hydrograph on the Tanana is dominated by melt of snowpack and glaciers during the spring and summer. Mean annual discharge for the open-water season (May to October) at the gauge at Nenana (station 15515500) from 1962 to 2015 is ~1299 m^3/s. The mean daily discharge on 9 June 2015 was 835 m^3/s, which is extremely low for that day of the year. For comparison, average discharge on 9 June from 1962 to 2015 is ~1220 m^3/s. The glacial origin of the Tanana River results in a high sediment load, which interacts with local topography to produce a complex morphology that ranges from highly braided to a single meandering channel [*Brabets et al.*, 2000]. This varied river morphology, in combination with ubiquitous sandbars and high bluffs (20–50 m high) along the study reach, makes this a challenging test site for AirSWOT's InSAR technology.

4. Methods

4.1. Field Methods

We conducted a 6 week field campaign from 15 May 2015 to 27 June 2015 to measure key hydrologic variables by using in situ and AirSWOT measurements along the Tanana River, AK (Figure 1). This paper's focus is on the 9 June 2015 AirSWOT data collection, which is currently the only date for which AirSWOT radar data have been fully processed, although we also use optical data from 17 June 2015 due to thin clouds present during the 9 June data collection. To assess AirSWOT's ability to measure river slopes and WSEs, we produced a high-resolution profile of WSEs. We used a Trimble R9 survey-grade GPS system attached to the back of a 8.5 m river boat to measure WSEs nearly continuously (0.5 s intervals; ~3 m spacing) along the main channel of the river on 7 June 2015 (Figure 1). In total, we collected 26,827 WSE measurements. In situ measurements were infeasible on 9 June due to logistical constraints, but hydraulic conditions were very similar between the two dates aside from a small decline in stage. Between 7 and 9 June, stage dropped 12 cm at Fairbanks and 17 cm at Nenana, resulting in a 0.05 cm/km difference in average slope between the two dates (24.80 cm/km on 7 June versus 24.85 cm/km on 9 June).

In addition to the GPS profile measurements of WSE, we installed a network of 20 Solinst Levelogger pressure transducers throughout the study reach to record temporal variations in stage every 2 min. Reported

accuracy for the pressure transducers at a maximum depth of 10 m is ±1 cm [http://www.solinst.com/products/dataloggers-and-telemetry/]. Eight of the 20 transducers are not considered here due to the instruments shifting or being buried by mobile sediment or collapsed riverbanks. This left 12 transducers available for analysis (Figure 1). We used static GPS surveys to convert the transducer stage values to WSEs by measuring the height difference between the water surface and the GPS-surveyed benchmarks using an optical survey level. The pressure transducers recorded similar declines in stage between 7 and 9 June compared to the USGS gauge measurements. Of the 12 transducers with viable stage measurements, eight were located on the main channel where the GPS profile measurements were collected. Changes in stage at the transducers located on the same channel as the GPS profile ranged from −15 cm to −20 cm, with an average difference of -17.8 cm and an average slope difference of 0.02 cm/km (23.98 cm/km on 7 June versus 24.00 cm/km on 9 June). Differences between slopes across the entire study reach calculated by using the USGS gauge stations and transducer sites are quite small (<0.05 cm/km) when compared to the reach average slope of ~24 cm/km. As a result, we subtracted the average stage difference calculated from the pressure transducers (−17.8 cm) from the 7 June profile observations to produce an estimated profile for 9 June that we compare to the AirSWOT measurements.

To achieve centimetric accuracies for the in situ WSE measurements, we used Natural Resources Canada's Canadian Geodetic Survey Precise Point Positioning tool for kinematic postprocessing of the GPS profile measurements and static postprocessing of GPS surveys conducted at the transducer sites [http://www.nrcan.gc.ca/earth-sciences/geomatics/geodetic-reference-systems/]. Vertical error estimates are not provided when processing kinematic measurements, so we estimated the random error for the profile elevations by applying a Gaussian filter to the profile and calculating the root-mean-square error (RMSE) between the raw measurements and smoothed profile. We chose a window of 100 points, which produces a smoothed profile that preserves sub-kilometer-scale features but eliminates noise. Larger smoothing windows result in convolution of signal (i.e., actual variations in WSE) with error and were thus avoided. RMSE between the smoothed profile and raw profile measurements is 2 cm, which is small compared to the anticipated AirSWOT measurement error. Elevation accuracies from the GPS surveys conducted at the transducer sites used to shift the profile are ±3.6 to ±6.4 cm. Given the combined pressure transducer instrument and survey errors (±1.5 cm), total uncertainty for the GPS profile increases to ±9.9 cm.

The AirSWOT flight on 9 June 2015 began at 7:52 A.M. and ended at 10:30 A.M. AirSWOT collected 21 swaths of elevation data, 9 swaths along a 43 km east region, and 12 swaths along a 32 km west region of the study area (Figure 1). The CIR camera on board the AirSWOT platform collected 1.16 m resolution optical photographs for each AirSWOT flight. Accurate location and orientation (latitude, longitude, altitude, roll, pitch, and heading) of the CIR camera at the instant of each image acquisition were obtained by using the AirSWOT platform Applanix GPS/IMU. Imagery was geo-rectified and processed into ortho-mosaics by using Agisoft PhotoScan software [http://www.agisoft.com/].

4.2. Remote Sensing Methods

The AirSWOT team at the NASA Jet Propulsion Laboratory (JPL), which processes the AirSWOT radar data, provided several data products for each AirSWOT line, all stored in flat binary files on regular grids. Data products used in this study include elevation in meters above the WGS84 ellipsoid, magnitude of the relative backscatter received by the sensor measured in decibels (dB), and estimated elevation error. Elevation errors are estimated from the phase variance (Cramer-Rao bound) which depends on the coherence between the two interferometric images [*Rosen et al.*, 2000]. Spatial resolution is 3.6 m for all binary files.

To extract WSEs from the radar imagery, we create a water mask from AirSWOT optical imagery using a binary threshold of 0.30 in the normalized difference water index transformation [*McFeeters*, 1996] (Figure S1 in the supporting information). Due to cloudy conditions on 9 June, we use optical imagery from 17 June to create the water mask. Water levels on 17 June were lower than those on 9 June (−22 cm), reducing the likelihood of land elevations being captured in the water mask but potentially resulting in the exclusion of some area inundated on 9 June. We multiply the AirSWOT elevation images by the optical water mask, which removes land pixels from analysis (Figure S2). There is potential for the chosen binary threshold to misclassify some land pixels as water in the mask, which would introduce error into the AirSWOT WSE images. Errors resulting from misclassified water/land pixels are likely minimal since water levels were slightly lower on the date used to create the water mask, and visual inspection of the water mask shows good agreement of water/land boundaries.

We apply a two-stage filtering process to refine the AirSWOT WSEs before comparing them to the field measurements (Figure S2). First, we use a ratio of magnitude divided by elevation error and exclude WSE pixels with ratios ≤5 dB of magnitude per meter of error. This threshold removes WSE pixels that are likely affected by layover and enforces stricter error limits on lower magnitude values. Since the magnitude decreases inside the swath, this method allows us to have a range-dependent threshold for the errors. Next, we use a moving 2 km^2 window to reduce remaining outliers by removing WSE pixels that are ±3 standard deviations away from the mean AirSWOT-derived elevation within the window. The remaining outliers are likely caused by misclassified water/land pixels from the water mask and poor ambiguity rejections at incidence angles <5° [*Goldstein et al.*, 1988]. On average, the filters eliminate 65% of the original WSE pixels in the east region and 39% of the original WSE pixels in the west region. When compared to the observed water mask area, the filtered elevations retain 84% of the water surface area in the east region and 95% of the water surface area in the west region due to overlap of AirSWOT measurement swaths. The filters eliminate more water pixels and area in the east region due to higher error values and lower magnitudes likely resulting from a combination of high adjacent topography and more complex channel morphology.

To determine AirSWOT WSE and slope errors, we compare the filtered AirSWOT WSEs to the GPS profile measurements. First, we calculate a mean AirSWOT elevation along a transect orthogonal to the GPS profile (Figure S3). We interpolate a 1 km orthogonal vector (±500 m) at each GPS profile measurement, extract the WSEs from the filtered AirSWOT images along this orthogonal, and average them together. Next, we segment the water mask in the downstream direction into 1 km^2 bins and average the AirSWOT WSEs and GPS profile measurements within each bin (Figure S3). We subtract the average AirSWOT WSEs from the average profile measurements in each bin to estimate the AirSWOT WSE error over 1 km^2 areas. We focus primarily on 1 km^2 bins because the SWOT science requirements are defined against this area, but we also test bin sizes ranging from 0.01 km^2 to 10 km^2. Finally, we calculate slopes from AirSWOT and GPS profile data by using a moving 10 km window that advances down the profile every 100 m. For each 10 km reach, we calculate slopes for both AirSWOT orthogonal mean values and the GPS profile measurements using linear regressions, then subtract the AirSWOT slopes from the GPS profile slopes. To assess AirSWOT's ability to capture slope variability, we compute Nash-Sutcliffe efficiency (NSE) values of the AirSWOT slopes relative to the GPS-derived slopes for the east and west regions [*McCuen et al.*, 2006]. NSE values range from −∞ to 1, with an NSE of 1 indicating that the GPS and AirSWOT slopes are identical and an NSE less than zero indicating that the mean GPS profile slope better characterizes slope variability than do the AirSWOT measurements. We also assess AirSWOT slope measurement capabilities along reach lengths ranging from 1 to 20 km using both RMSE and NSE.

5. Results

Comparison of AirSWOT and in situ WSE profiles shows strong similarities between the measurements. Figure 2 shows the orthogonal means of AirSWOT WSEs and the GPS WSE profiles for the east (Figure 2a) and west (Figure 2b) regions. The majority (73%) of WSE errors within 1 km^2 regions fall below the science requirements defined by the SWOT mission of ±10 cm, with an RMSE of 9.0 cm and mean absolute error (MAE) of 7.1 cm (Figure 2c). Bias, at 0.65 cm, is a very small component of AirSWOT measurement error relative to in situ observations. The largest AirSWOT WSE deviations from the observations occur in the first 10 km of both the east and west regions. WSE errors vary with the size of the averaging bins, with higher errors at smaller bin sizes (Figure S4a). Given the uncertainty in the GPS profile measurements (±9.9 cm), observational uncertainty likely accounts for a substantial portion of the AirSWOT WSE errors.

For 10 km reach lengths, AirSWOT is capable of accurately measuring slopes with an RMSE of 1.0 cm/km, as well as capturing detailed variations in slopes, with NSE values of 0.76 and 0.93 for the east and west regions, respectively. Figure 3 shows slopes along 10 km reaches for the east (Figure 3a) and west regions (Figure 3b). Out of 499 overlapping 10 km reaches (289 east and 210 west), 90% of slope errors are at or below the SWOT science requirements of ±1.7 cm/km (Figure 3c). Slope errors range from −2.4 cm/km to 2.2 cm/km, with an RMSE of 1.0 cm/km and an MAE of 0.83 cm/km. Slope errors decline predictably with reach length, from 17.8 cm/km for 1 km reaches to 0.6 cm/km for 20 km reaches (Figure S4b). NSE values are generally lower for shorter reaches, although the increase is not monotonic with reach length (Figure S5). Slopes with errors greater than the SWOT science requirement are likely affected by topographic layover from high bluffs adjacent to the channel (Figure 2) and incorrect ambiguity heights. Ambiguity heights are used in InSAR
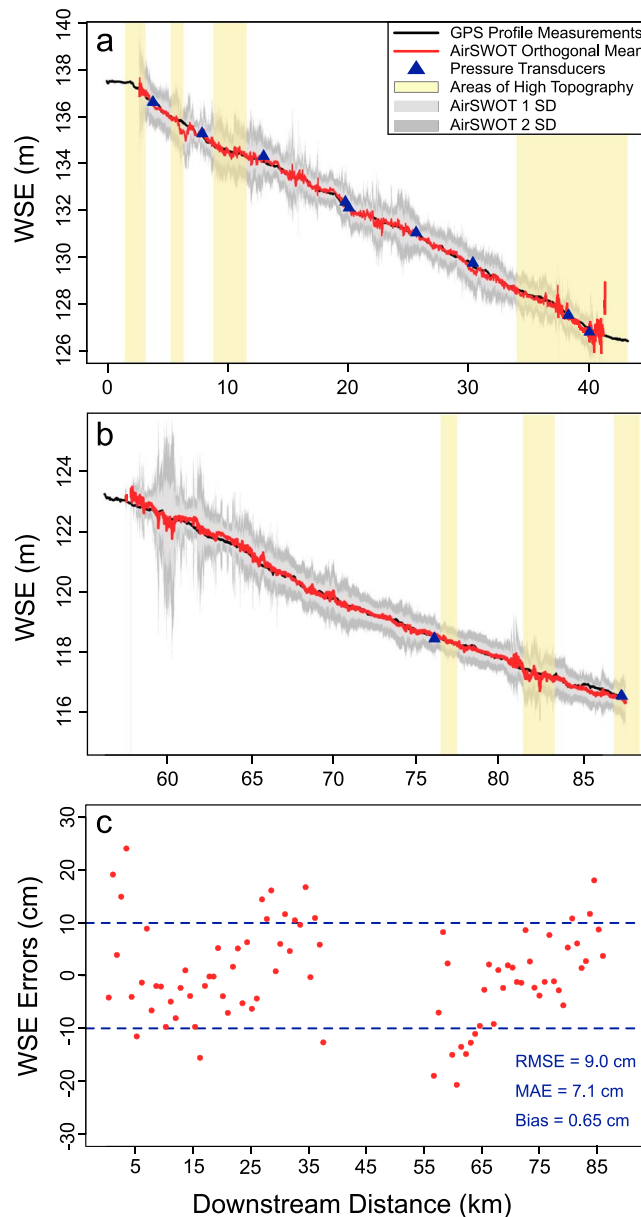
Figure 2. WSE profiles derived from GPS (black) and AirSWOT (red) for the (a) east and (b) west regions. Standard deviations (SD) are shown for the AirSWOT WSEs in the grey shaded areas. (c) Differences between GPS WSEs and AirSWOT WSEs averaged over 1 km² areas. The blue dashed lines mark the SWOT science requirement for WSE accuracies (±10 cm).

processing to unwrap the interferometric phase, an important step in retrieving the elevations, and are sensitive to areas of high topography as well as aircraft pitch and roll [*Rosen et al.*, 2000]. Therefore, incorrect ambiguity heights may lead to large errors in elevation measurements. Additionally, some portion of the difference between the AirSWOT and GPS profile slopes could be attributable to slope changes that may have occurred between 7 June, when the in situ measurements were collected, and the 9 June AirSWOT flight.

6. Discussion

AirSWOT provides a new, robust method for measuring WSEs and slopes over considerable reach lengths without the need for in situ data. Results indicate that AirSWOT accuracies are high enough to capture decimeter-level variations in WSEs with estimated errors at or below 10 cm when averaged over areas ≥ 0.49 km² (Figures 2 and S4a). We observe a mean bias in averaged AirSWOT WSEs of <1 cm without any intercalibration between in situ and AirSWOT measurements. Furthermore, AirSWOT measurements are capable of capturing centimeter-per-kilometer-level variations in slopes with an RMSE of 1.0 cm/km for 10 km reaches (Figure 3) and an RMSE as low 0.6 cm/km for 20 km reaches (Figure S4b). There are no previous airborne or satellite missions that like AirSWOT, use short (Ka-band) wavelength radar measurements acquired at low-incidence angles to measure rivers. As a result, while AirSWOT processing is similar to other InSAR methodologies, new procedures for handling the complexities
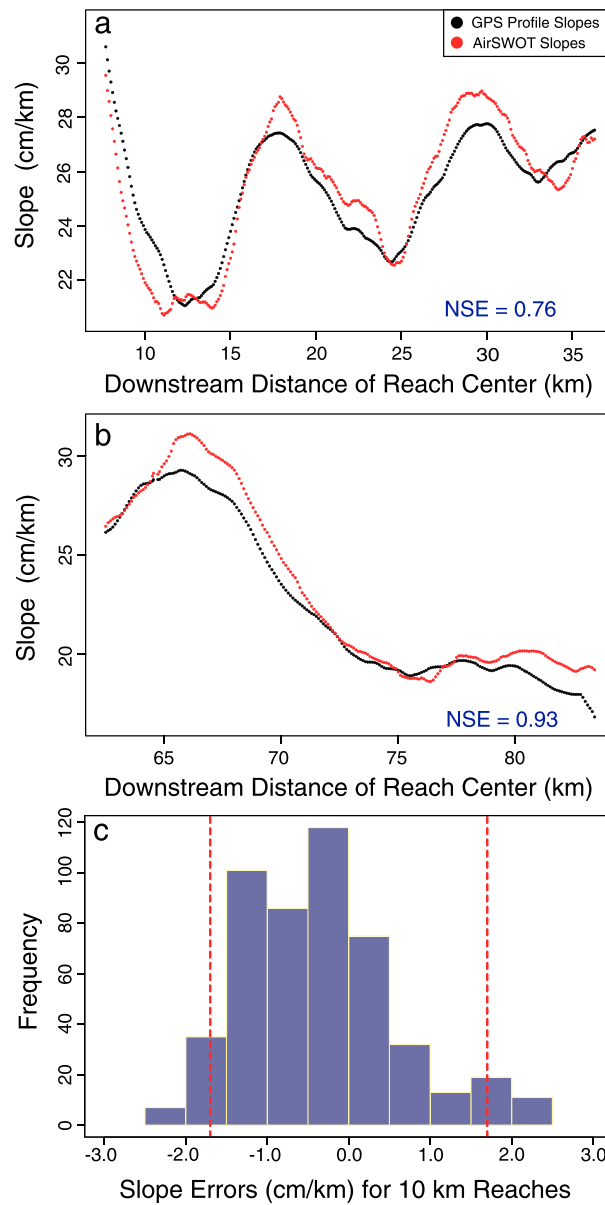
arising during calibration remain under development and may account for some of the observed error. Despite current processing limitations, AirSWOT provides unprecedented remotely sensed measurements of river WSE and slope even in a challenging river environment like the Tanana.

The impressive details observed by AirSWOT offer new opportunities to explore surface water hydrology. Future studies can use AirSWOT to characterize spatial controls on regional stream hydraulics at comparatively fine spatial and temporal resolutions. SWOT is expressly designed to observe surface water dynamics, but it will have significant gaps in spatial coverage, with 2–10 revisits per 21 day orbit cycle and will only observe rivers wider than 50–100 m [*Biancamaria et al.*, 2016b]. These characteristics limit SWOT observations of surface water fluxes to weekly and monthly timescales, which can miss the peaks and troughs of rapid

Figure 3. Slopes from GPS profile and AirSWOT for the 499 overlapping 10 km reaches within the (a) east and (b) west regions versus the center of each reach in order of downstream distance. Successive reach segments are shifted downstream by 100 m. (c) Histogram of slope errors for AirSWOT slopes relative to GPS-derived measurements. The red dashed lines mark the SWOT science requirement for slope accuracies (±1.7 cm/km).

hydrologic events. In contrast, AirSWOT can be tasked to take repeat measurements across hundreds of kilometers of river reaches at hourly or daily timescales. These measurements can be used to observe detailed passages of flood waves and provide estimates of WSE and slope variability between existing in situ gauges or altimeter measurements to help understand spatial controls on river hydraulics [*Garambois et al.*, 2016]. Additionally, AirSWOT's fine spatial resolution (<4 m) allows for better visibility in small river systems that play a nonnegligible role in the water and carbon cycles and are poorly gauged or not observable by satellites [*Raymond et al.*, 2013; *Biancamaria et al.*, 2016a]. AirSWOT measurements can be spatially averaged to get WSE and slope estimates in rivers with widths <50 m. AirSWOT measurements are also valuable for distributed hydrological analysis in highly multidimensional systems, such as braided rivers and deltas, where spatially distributed in situ observations are difficult to attain and tidal effects require fine temporal resolution measurements [*Wolski et al.*, 2006; *Schubert et al.*, 2015].

AirSWOT measurements can be a powerful tool to enhance flood models. Hydrodynamic models suffer from a lack of spatially distributed calibration and validation data and are often constrained by point measurements of WSE from ground campaigns, altimeters, or gauge stations. These data constraints limit the capabilities of models by admitting many "optimal" parameter combinations during calibration [*Pappenberger et al.*, 2005; *Hunter et al.*, 2007; *Bates et al.*, 2013]. Scientists can use AirSWOT measurements to constrain model parameters over long reach distances and to improve understanding of the physical processes controlling the spatial distribution of model parameters [*Hall et al.*, 2005; *Warmink et al.*, 2013]. AirSWOT measurements can also be used to validate models' abilities to reproduce spatial variations in slope across hundreds of kilometers and can be assimilated to improve model accuracies. Additionally, AirSWOT is capable of acquiring measurements in cloudy conditions and can be assigned to take measurements during critical hydraulic events (e. g. after a storm) to capture flood peaks and maximum inundation extents that are often missed by existing satellite sensors [*Biancamaria et al.*, 2016a]. These measurements can enable better model calibration and validation, allowing improved prediction of areas vulnerable to flooding.

Finally, these results support the use of AirSWOT as a future validation instrument for SWOT. The results of this study show that AirSWOT is capable of producing SWOT-quality or better measurements of river WSEs

and slopes. Considering lower errors are expected at lower incidence angles, these errors are likely to decrease as processing methods advance and AirSWOT data at SWOT-like incidence angles can be included. In addition to SWOT validation, other ongoing projects are using AirSWOT data to help determine the effects on radar returns of specular water surfaces associated with low wind speeds, better quantify the frequency and extent of topographic layover effects, and assess returns from inundated vegetation [*Biancamaria et al.*, 2016b]. The results of this study present the first published demonstration of AirSWOT's ability to accurately measure WSEs and slopes and its promise as a future validation instrument for the SWOT mission. Future work should seek to validate AirSWOT's ability to measure 2-D slopes in floodplain environments, to characterize AirSWOT's accuracy across a variety of river sizes and morphologies, and to understand AirSWOT's abilities to measure WSEs in lakes and wetlands.

References

Alsdorf, D. E., E. Rodríguez, and D. P. Lettenmaier (2007b), Measuring surface water from space, *Rev. Geophys.*, *45*, RG2002, doi:10.1029/2006RG000197.

Alsdorf, D., P. Bates, J. Melack, M. Wilson, and T. Dunne (2007a), Spatial and temporal complexity of the Amazon flood measured from space, *Geophys. Res. Lett.*, *34*, L08402, doi:10.1029/2007GL029447.

Bates, P. D. (2012), Integrating remote sensing data with flood inundation models: how far have we got?, *Hydrol. Process.*, *26*(16), 2515–2521, doi:10.1002/hyp.9374.

Bates, P. D., F. Pappenberger, and R. J. Romanowicz (2013), Uncertainty in flood inundation modelling, in *Applied uncertainty analysis for flood risk management*, edited by K. Beven and J. Hall, pp. 232–269 , Imperial College Press, Singapore.

Bates, P. D., J. C. Neal, D. Alsdorf, and G. J. P. Schumann (2014), Observing global surface water flood dynamics, *Surv. Geophys.*, *35*(3), 839–852, doi:10.1007/s10712-013-9269-4.

Biancamaria, S., F. Frappart, A. S. Leleu, V. Marieu, D. Blumstein, J. D. Desjonquères, F. Boy, A. Sottolichio, and A. Valle-Levinson (2016a), Satellite radar altimetry water elevations performance over a 200 m wide river: Evaluation over the Garonne River, *Adv. Space Res.*, doi:10.1016/j.asr.2016.10.008.

Biancamaria, S., D. P. Lettenmaier, and T. M. Pavelsky (2016b), The SWOT mission and its capabilities for land hydrology, *Surv. Geophys.*, *37*, 307–337, doi:10.1007/s10712-015-9346-y.

Brabets, T. P., B. Wang, and R. H. Meade (2000), Environmental and hydrologic overview of the Yukon River Basin, Alaska and Canada, *US Dep. Inter. US Geol. Surv.*

Calmant, S., F. Seyler, and J. F. Cretaux (2008), Monitoring continental surface waters by satellite altimetry, *Surv. Geophys.*, *29*(4-5), 247–269, doi:10.1007/s10712-008-9051-1.

Clark, E. A., J. Sheffield, M. T. H. van Vliet, B. Nijssen, and D. P. Lettenmaier (2015), Continental runoff into the oceans (1950–2008), *J. Hydrometeorol.*, *16*(4), 1502–1520, doi:10.1175/JHM-D-14-0183.1.

Di Baldassarre, G., and S. Uhlenbrook (2012), Is the current flood of data enough? A treatise on research needs for the improvement of flood modelling, *Hydrol. Process.*, *26*(1), 153–158, doi:10.1002/hyp.8226.

Durand, M., et al. (2016), An intercomparison of remote sensing river discharge estimation algorithms from measurements of river height, width, and slope, *Water Resour. Res.*, *52*(6), 4527–4549, doi:10.1002/2015WR018434.

Enjolras, V. M., and E. Rodriguez (2009), An assessment of a Ka-band radar interferometer mission accuracy over Eurasian Rivers, *IEEE Transactions on Geoscience and Remote Sensing*, *47*(6), 1752–1765, doi:10.1109/TGRS.2008.2006370.

Famiglietti, J. S., and M. Rodell (2013), Water in the balance, *Science*, *340*(6138), 1300–1301, doi:10.1126/science.1236460.

Fjørtoft, R., et al. (2014), KaRIn on SWOT: Characteristics of near-nadir Ka-band interferometric SAR imagery, *IEEE Trans. Geosci. Remote Sens.*, *52*(4), 2172–2185, doi:10.1109/TGRS.2013.2258402.

Fu L. L., D. E. Alsdorf, R. Morrow, E. Rodriguez, N. M. Mognard (2012) SWOT: The Surface Water and Ocean Topography mission. *JPL Publication 12 05*. [Available at http://swot.jpl.nasa.gov/files/swot/SWOT_MSD_1202012.pdf.]

Garambois, P. A., S. Calmant, H. Roux, A. Paris, J. Monnier, P. Finaud-Guyot, A. Montazem, and J. Santos da Silva (2016), Hydraulic visibility: using satellite altimetry to parameterize a hydraulic model of an ungauged reach of a braided river, *Hydrol. Process.*, 1–20, doi:10.1002/hyp.11033.

Goldstein, R. M., H. A. Zebker, and C. L. Werner (1988), Satellite radar interferometry: Two-dimensional phase unwrapping, *Radio Sci.*, *23*(4), 713–720, doi:10.1029/RS023i004p00713.

Hall, J. W., S. Tarantola, P. D. Bates, and M. S. Horritt (2005), Distributed sensitivity analysis of flood inundation model calibration, *Journal of Hydraulic Engineering*, *131*(2), 117–126, doi:10.1061/(ASCE)0733-9429(2005)131:2(117).

Hannah, D. M., S. Demuth, H. A. J. van Lanen, U. Looser, C. Prudhomme, G. Rees, K. Stahl, and L. M. Tallaksen (2011), Large-scale river flow archives: Importance, current status and future needs, *Hydrol. Process.*, *25*(7), 1191–1200, doi:10.1002/hyp.7794.

Hunter, N. M., P. D. Bates, M. S. Horritt, and M. D. Wilson (2007), Simple spatially-distributed models for predicting flood inundation: A review, *Geomorphology*, *90*(3–4), 208–225, doi:10.1016/j.geomorph.2006.10.021.

Marcus, W. A., and M. A. Fonstad (2008), Optical remote mapping of rivers at sub-meter resolutions and watershed extents, *Earth Surf. Process. Landforms*, *33*(1), 4–24, doi:10.1002/esp.

McCuen, R. H., Z. Knight, and A. G. Cutter (2006), Evaluation of the Nash–Sutcliffe efficiency index, *J. Hydrol. Eng.*, *11*(6), 597–602, doi:10.1061/(ASCE)1084-0699(2006)11:6(597).

McFeeters, S. K. (1996), The use of the normalized difference water index (NDWI) in the delineation of open water features, *Int. J. Remote Sens.*, *17*(7), 1425–1432, doi:10.1080/01431169608948714.

Moller, D., E. Rodriguez, J. Carswell, and D. Esteban-Fernandez (2011), AirSWOT—A calibration/validation platform for the SWOT mission, in *Proc. Interntational Geoscience and Remote Sensing Symposium*, Vancouver, Canada.

O'Loughlin, F. E., J. Neal, D. Yamazaki, and P. D. Bates (2016), ICESat-derived inland water surface spot heights, *Water Resour. Res.*, *52*(4), 3276–3284, doi:10.1002/2014WR015716.

O'Loughlin, F., M. A. Trigg, G. J. P. Schumann, and P. D. Bates (2013), Hydraulic characterization of the middle reach of the Congo River, *Water Resour. Res.*, *49*(8), 5059–5070, doi:10.1002/wrcr.20398.

Pappenberger, F., K. Beven, M. Horritt, and S. Blazkova (2005), Uncertainty in the calibration of effective roughness parameters in HEC-RAS using inundation and downstream level observations, *J. Hydrol.*, *302*(1–4), 46–69, doi:10.1016/j.jhydrol.2004.06.036.

Paris, A., R. C. Paiva, J. S. Silva, D. M. Moreira, S. Calmant, P. A. Garambois, W. Collischonn, M. P. Bonnet, and F. Seyler (2016), Stage-discharge rating curves based on satellite altimetry and modeled discharge in the Amazon basin, *Water Resour. Res.*, *25*(16), 3447–3459, doi:10.1002/2014WR015716.

Pavelsky, T. M., M. T. Durand, K. M. Andreadis, R. E. Beighley, R. C. Paiva, G. H. Allen, and Z. F. Miller (2014), Assessing the potential global extent of SWOT river discharge observations, *J. Hydrol.*, *519*, 1516–1525, doi:10.1016/j.jhydrol.2014.08.044.

Raymond, P. A., et al. (2013), Global carbon dioxide emissions from inland waters, *Nature*, *503*(7476), 355–359, doi:10.1038/nature12760.

Rodell, M., et al. (2015), The observed state of the water cycle in the early twenty-first century, *J. Clim.*, *28*(21), 8289–8318, doi:10.1175/JCLI-D-14-00555.1.

Rodriguez, E. (2016), Surface Water and Ocean Topography Mission (SWOT). *Science requirements Document V1*, 1.

Rosen, P. A., S. Hensley, I. R. Joughin, F. K. Li, S. N. Madsen, E. Rodriguez, and R. M. Goldstein (2000), Synthetic aperture radar interferometry, *Proc. IEEE*, *88*(3), 333–382, doi:10.1088/0266-5611/14/4/001.

Schubert, J. E., W. W. Monsen, and B. F. Sanders (2015), Metric-resolution 2D river modeling at the macroscale: Computational methods and applications in a braided river, *Front. Earth Sci.*, *3*, 74, doi:10.3389/feart.2015.00074.

Schumann, G. J. P., P. D. Bates, M. S. Horritt, P. Matgen, and F. Pappenberger (2009), Progress in integration of remote sensing-derived flood extent and stage data and hydraulic models, *Rev. Geophys.*, *47*, RG4001, doi:10.1029/2008RG000274.

Smith, L. C. (1997), Satellite remote sensing of river inundation area, stage, and discharge: A review, *Hydrol. Process.*, *11*(10), 1427–1439, doi:10.1002/(SICI)1099-1085(199708)11:10<1427::AID-HYP473>3.3.CO;2-J.

Warmink, J. J., M. J. Booij, H. Van der Klis, and S. J. M. H. Hulscher (2013), Quantification of uncertainty in design water levels due to uncertain bed form roughness in the Dutch river Waal, *Hydrol. Process.*, *27*(11), 1646–1663, doi:10.1002/hyp.9319.

Wolski, P., H. H. G. Savenije, M. Murray-Hudson, and T. Gumbricht (2006), Modelling of the flooding in the Okavango Delta, Botswana, using a hybrid reservoir-GIS model, *J. Hydrol.*, *331*(1), 58–72, doi:10.1016/j.jhydrol.2006.04.040.